Long-term trends and projections of hydrological fluxes under RCP climate change scenarios for a mountainous river catchment of northeast India

S. Murasingh[a], J. Kuttippurath [iD][a,*], S. Sandeep Dash[b], S. Raj[a], R. Remesan[b], Madan K. Jha[c] and P. Kumar[a]

[a] CORAL, Indian Institute of Technology Kharagpur, 721 302 Kharagpur, India
[b] School of Water Resources, Indian Institute of Technology Kharagpur, Kharagpur, India
[c] AgFE Department, Indian Institute of Technology Kharagpur, Kharagpur, India
*Corresponding author. E-mail: jayan@coral.iitkgp.ac.in

[iD] JK, 0000-0003-4073-8918

ABSTRACT

The estimate of changes in hydrological fluxes from a climate change perspective is inevitable for assessing the sustainability of watersheds and conserving water resources. Here, we quantify and assess the changes in different hydrological flux components for the Manu-Deo River Basin (MDRB) of northeast India using Soil and Water Assessment Tool (SWAT) simulations and multi-temporal data at various resolutions. Sequential Uncertainty Fitting (SUFI-2) optimization is used to calibrate and validate the simulations for the periods 1984–2006 and 2007–2016 and for the four future representative concentration pathway (RCP) scenarios. The model performed reasonably well for the calibration and validation of daily data, in accordance with the Nash–Sutcliffe efficiency and coefficient of determination (0.54/0.55 and 0.52/0.72, respectively). The analysis for the period 1985–2013 reveals a decreasing trend in streamflow, which indicates increasing trends of drought there. Furthermore, it shows an increasing trend in evapotranspiration (ET) and decreasing trend for baseflow (BF), suggesting an adverse impact on agricultural production during lean periods. In addition, the RCP 2.6 and 6.0 scenarios for the monsoon season in future time scales are expected to cause a reduction in different flow components, although RCP 8.5 shows increased water availability there. The sub-basin-scale quantification and multi-temporal analysis of water availability under the present and future climate scenarios, as presented here, can assist water managers in formulating a suitable operational policy to implement a better decision-making framework for river and waterbody management. This is particularly important for mountainous regions, where input data are sparse and modelling of hydrological fluxes is challenging.

Key words: climate change, hydrological fluxes, linear trends, northeast India, RCP scenarios, SWAT

HIGHLIGHTS

- A model for a mountain river basin is customized to analyse hydrological fluxes.
- The model performs better at a monthly time scale than at a daily time scale.
- Streamflow has been decreasing in the basin but increases in all RCP scenarios.
- Increase in evapotranspiration in monsoon seasons in both past and future periods.
- A multi-model approach provides more reliable estimates of water balance components.

GRAPHICAL ABSTRACT
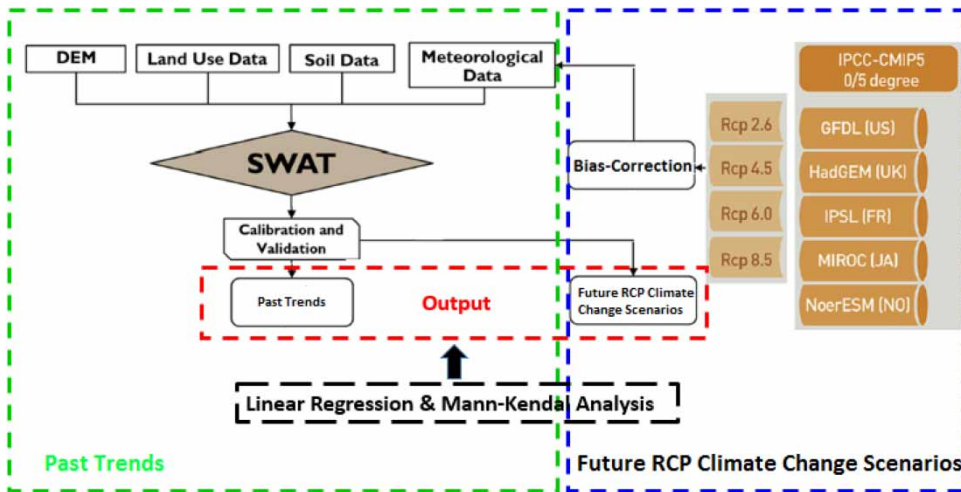
1. INTRODUCTION

Hydrological modelling stands as a suitable tool for quantitative analysis of water resources. Nevertheless, the availability of appropriate hydro-meteorological inputs and suitable hydrological model selection would decide model performance (Dash *et al.* 2021). The hydrological cycle is more dynamic and highly susceptible to frequent alterations in the magnitude of different water balance components. Furthermore, an accurate quantification of available water resources is highly essential, which is particularly important in mountainous regions. Nevertheless, the remote location of a mountain region leads to poor availability of model input data, which makes the hydrological modelling process very difficult and intricate.

There are several hydrological modelling initiatives, ranging from the lumped black-box model, artificial neural network (ANN) to the distributed MIKE-SHE model. The lumped black-box models are subject to larger uncertainties due to inadequate representation of basin characteristics and hydrological processes in their modelling process. Conversely, the physically based modelling approach is limited to input data availability and detailed basin information. In this context, the Soil and Water Assessment Tool (SWAT) is a good alternative that focuses on the basin-scale assessment of streamflow, evapotranspiration (ET), groundwater recharge and baseflow (BF; Arnold *et al.* 1993, 2000). This model has also been useful for diagnosing the effect of global warming on long-term water availability and nutrient and sediment loading (Padhiary *et al.* 2020). Although the SWAT model is recognized internationally as a powerful interdisciplinary tool for watershed management, relatively few studies have been conducted for northeast India with mountainous terrains, and hydrological simulations for such regions are complex and challenging.

Northeast India is considered as the wettest region on earth with heavy rainfall in summer or during the southwest monsoon (Kuttippurath *et al.* 2021). An increased number of heavy rainfall events have produced frequent floods there (Singh & Kumar 2013), and the annual rainfall has increased by 3.72 mm/year in the hilly regions of the northeast, although this rate is not statistically significant (Varikoden & Revadekar 2020). Choudhury *et al.* (2012) reported a marginal drop in rainfall in monsoon months, with about 1.7 mm/year. The most recent study also points out that there is a substantial decrease in rainfall across the northeast regions, which has shifted the wettest place on earth to Mawsynram from Cherrapunji (Kuttippurath *et al.* 2021). The decrease in rainfall can affect the hydrology of the region and, therefore, demands modelling of hydrological fluxes to analyse past trends and future projections.

The global rise in temperature and unpredictability in precipitation across different spatial–temporal scales are major concerns, and this variability in climate is likely to intensify in the coming century (Kharin *et al.* 2013). Furthermore, climate change may affect the basin-wide hydrology through changes in the precipitation characteristics (e.g., Sinha *et al.* 2020). Therefore, an assessment of basin hydrological behaviour and subsequent estimates of water balance components are inevitable in the wake of global warming. Hydrological models could be a good alternative in assessing the water balance of watersheds, although validation and calibration are very difficult in mountainous regions such as northeast India, due to the inherent natural randomness, and data, model and operational uncertainties (Tung 2005).

SWAT can be calibrated with a trial-and-error approach or using an auto-calibration technique, SWAT-CUP (SWAT Calibration and Uncertainty Programs). As the watershed-scale model involves a higher number of parameters for calibration, it is common in hydrological studies to use automated calibration tools involving certain optimization techniques (Murasingh *et al.* 2018). Therefore, it would be imperative to examine the impact of changes in climate on regional scales at which management decisions are to be taken. For instance, earlier studies on smaller basins (i.e., <10,000 km² area) were performed for the Upper Baitarani River Basin (Dhar & Mazumdar 2009; Raneesh & Santosh 2011; Verma & Jha 2015). Studies on small basins are few, and those on the northeast regions are also limited (Kusre *et al.* 2010; Goyal *et al.* 2018), suggesting the importance of this study.

The Manu-Deo River Basin (MDRB) has rubber plantations, agricultural land (paddy), and semi-urban development that require a substantial amount of water. The rapid development in agriculture and increased deforestation have consequences on the MDRB environment. The MDRB has surface and groundwater availability issues because it is a medium-scale river basin in a hilly region. Therefore, climate change could have an impact on the hydrology of the MDRB. Here, we analyse the long-term changes in climate variables, assess the efficiency of the SWAT model in mountainous basins and estimate the changes in hydrological fluxes for the future representative concentration pathway (RCP) scenarios. The MDRB's historical and future trends of mean annual and seasonal fluxes are studied using a multi-temporal approach based on linear regression and the Mann–Kendall test.

2. DATA AND METHODOLOGY

2.1. Area of the study

The MDRB (2,278 km²) is a sub-basin of Barak and other basins that lies between 23°39′ and 24°22′N and 91°54′ and 92°16′E (Figure 1). The MDRB is characterized by a combination of two major perennial rivers, i.e., Manu and Deo, that originate from the hills of northeast India. River Deo is the main tributary of river Manu, which runs through 132 km before meeting Manu near Kumarghat. The Manu River originates from the Sakhan range, flows parallel to the Deo River and joins the Meghna River in Bangladesh, with a total length of about 167 km in India. About 88.8% (2,023 km²) of the MDRB lies in the hilly region and about 11.2% (255 km²) in the plains (Bhattacharya 2017). The MDRB exhibits high topographical variation as envisaged from its elevation ranging from 4 to 945 m. The basin is characterized by a humid subtropical climate and it receives an annual rainfall of 1,500–2,500 mm, 62% of which is from the southwest monsoon. The occurrence of heavy rainfall during the monsoon season causes frequent floods and related damage in the area. Occasional pre-monsoon rainfall is also found during the last week of March to mid-April there, and this is termed 'Kal Baishakhi'.

A rapid increase in temperature is observed from March, and the highest monthly temperature is found in June, which is about 30 °C, whereas the lowest monthly temperature is observed in January, which is about 16 °C. Naturally grown forests of the MDRB are mostly characterized by bamboo plants. Nearly 65.83% of the MDRB area is covered with forest, and the floodplain is predominantly used for agriculture. Lateritic soil is found in the hilly areas and river valleys, but younger
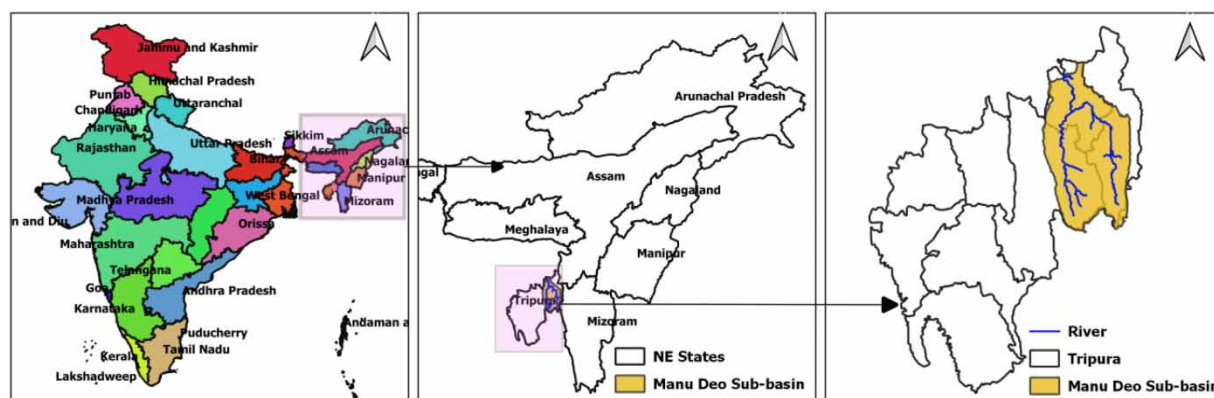

Figure 1 | India map (left), northeast India (middle) and Tripura state with the river basin selected for this study.

soils are found in the floodplain of all major 'Tuisa' (local name for 'stream') and clay soils in the paddy fields. The dominant soil texture of the MDRB is the residual, transported and lateritic (Supplementary Table S1).

2.2. Pedo-hydrologic database

Soil map, land use land cover (LULC) and digital elevation model (DEM) are the primary inputs to the SWAT model. In addition, temporal information on meteorological parameters and stream discharge (streamflow) is required. Supplementary Table S2 lists data procured from different sources. The DEM of the area was obtained from the Shuttle Radar Topographic Mission (SRTM) DEM (30 m×30 m). A cloud-free satellite image (Landsat ETM+ imagery) for 25 December 2008, having path 136 and rows 43, with 44 of 30 m spatial resolution, is used to make the LULC map. The Landsat imageries were classified (supervised) into six LULC classes using ERDAS IMAGINE 2014 software. The daily rainfall, temperature (T_{max} and T_{min}) and other meteorological parameters for the period 1980–2016 were obtained from the India Meteorological Department station located at Kailashahar. Similarly, the daily streamflow measured at the Kailashahar gauge station for the same period was taken from the Central Water Commission, Assam. We used RCP 8.5, 6, 4.5 and 2 scenario simulations from five different GCMs: NorESM1-M, GFDL-ESM2M, MIROC-ESM-CHEM, IPSL-CM5A-LR and HadGEM2-ES (Moss *et al.* 2010) (Supplementary Table S3).

2.3. Methodology

2.3.1. SWAT model

The ArcGIS 10.1 interface of SWAT (version 2012) is used in this study, which is commonly known as ArcSWAT. The model simulates the hydrological cycle based on water balance (Neitsch *et al.* 2011):

$$SWC_t = SWC_0 + \sum_{t=1}^{t} (P_{day} - Q_{Surface\ Runoff} - ET - I - G_w) \tag{1}$$

where SWC_t (mm/day) is the soil water content (final), and SWC_0 (mm/day) is the initial soil water content on day t, t (days) is the time, P_{day} is the amount of precipitation (on day t), $Q_{surface\ Runoff}$ is the amount of surface runoff (on day t), ET (mm/day) is the amount of evapotranspiration (on day t), I (mm/day) is the amount of percolated water (on day t) and G_w is the amount of return flow (on day t). Hydrology, weather, soil temperature, crop growth, nutrients, bacteria and land management are the major modelling components of SWAT. In the hydrologic response unit (HRU) scale, the model performs the simulation of different process components such as streamflow, sediment yield and pollutant loading. The HRUs are treated as the sole combinations of soil classes, land-use type and slope condition. The study area is divided into 29 sub-basins, which are further discretized into 640 HRUs that effectively represent the watershed heterogeneity.

2.3.2. Sensitivity analysis of ArcSWAT

SWAT includes over 200 parameters, wherein a large percentage does not affect the model output significantly. In this context, it is essential to select the appropriate model parameters for streamflow simulations. This step certainly helps in the sorting of a number of calibration parameters, and subsequently, gives an overview of the model parameter selection and handling. The calibration and validation of streamflow simulations were done using the observed flow time series for the periods 1984–2006 and 2007–2016, respectively. The beginning 4-year period, i.e., 1980–1983, was treated as the spin-up time, so that model initial conditions could be stabilized.

The model performance is generally evaluated by using different goodness-of-fit indicators such as the R^2 and the Nash–Sutcliffe efficiency (NSE). In addition, the percent bias (PBIAS) is also considered, which provides an overview of whether the model error lies within the acceptable limit or not. The corresponding equations of the above-said goodness-of-fit indicators are given below:

$$NSE = 1 - \frac{\sum_{i=1}^{n} (O_i - P_i)^2}{\sum_{i=1}^{n} (O_i - O')^2} \tag{2}$$

R^2, which ranges from 0 to 1, is used to check the co-linearity between simulated and observed streamflow values.

$$R^2 = \left\{ \frac{\left(\sum\limits_{i=1}^{n} (O_i - O')(P_i - P') \right)^2}{\sum\limits_{i=1}^{n} (O_i - O')^2 \sum\limits_{i=1}^{n} (P_i - P')^2} \right\} \tag{3}$$

$$PBIAS = \frac{\sum\limits_{i=1}^{n} (O_i - P_i)}{\sum\limits_{i=1}^{n} O_i} \times 100 \tag{4}$$

where n is the total number of data, O_i and P_i are the observed and simulated data at time i and O' and P' are the mean of observed and simulated data. Still closer to the values of the *NSE* and R^2 to 1, the model tends to perform better, and better captures the dynamics. The *NSE* generally lies between $-\infty$ and 1, with positive values indicating that the model reproduced the observed changes with less uncertainty. However, a PBIAS estimate of -25 to $+25\%$ corresponds to acceptable model section criteria in hydrological modelling (Dash *et al.* 2019).

2.3.3. Pre-processing of climatological data

We use five GCMs for analysing the future climate scenarios over the MDRB as listed in Supplementary Table S3. Therefore, all GCM output data are downscaled to a common resolution of 0.5°×0.5° prior to the future hydrological quantification. Because of the random and systematic model errors, a bias correction of the GCM output is quite essential (Teutschbein & Seibert 2010; Fiseha *et al.* 2014). Both parametric and non-parametric bias correction methods, as shown in Supplementary Figure S1, can be used to reduce the existing bias in meteorological variables. The mountain regions experience orographic precipitation with variable intensities at different elevations. Therefore, the usual downscaling approach adopted in plain regions may not adequately represent the variability of precipitation in the mountainous regions (e.g., Praskievicz 2018). To deal with this situation, we adopted the local topographic lapse rate (LTLR)-based downscaling method proposed by Praskievicz & Bartlein (2014). Time series of precipitation, and the maximum and minimum temperatures were extracted from the LTLR-downscaled and localized constructed analogs (LOCA) downscaled grid cell that includes each station. Probability density function (PDF) skill scores were then calculated for the LOCA and LTLR-downscaled data using the observed time series at each station:

$$S_{score} = \sum_{1}^{n} \text{minimum}(Z_m, Z_0)$$

where S_{score} is the skill score, n is the number of bins used to calculate the PDF, Z_m is the frequency of modelled values in a given bin and Z_0 is the frequency of observed values in a given bin. If the forecast were perfect, the skill score would be 1 because the PDFs of the observed and modelled values would completely overlap, whereas a little overlap between those data would result in a low skill score near 0.

2.3.4. Spatiotemporal quantification of hydrological fluxes

We have considered five different hydrological fluxes, namely, streamflow (Q), ET, BF, shallow aquifer recharge (SAR) and deep aquifer recharge (DAR), for the assessment. The relative variation in the hydrological fluxes over a longer time scale was analysed using the parametric and non-parametric trend analysis as detailed below.

Simple regression is a parametric statistical technique that has been extensively used for identifying the direction and rate of change that occur in a long-term time series. The simple linear regression model is expressed as follows:

$$Y = mX + c \tag{5}$$

where Y is the rainfall, X is the time step in a year, m is the average rate of change of rainfall per year and c is the y-intercept. The rate of change with respect to time is indicated by m, and the sign of the slope defines its direction. A positive sign is used to indicate increase and a negative sign is for decrease.

The Mann–Kendall analysis (Mann 1945; Kendall 1975), also known as the MK test, is formulated as distribution:

$$Var(\text{S}) = \frac{1}{18}[n(n-1)(2n+5)] \tag{6}$$

where the size of data is given by n and Z statistic of Mann–Kendall analysis is computed as such:

$$Z_{calculated} = \begin{cases} \dfrac{S-1}{\sqrt{Var(\text{S})}} & \text{if } S > 0 \\ 0 & \text{if } S = 0 \\ \dfrac{S+1}{\sqrt{Var(\text{S})}} & \text{if } S < 0 \end{cases} \tag{7}$$

If the computed value of $Z_{calculated}$ is greater than $Z_{tabulated}$, it is a statistically significant trend and rejects the null hypothesis. The upward and downward trends in a time series are known by a positive or negative value of $Z_{calculated}$. For the present analysis, the level of significance, i.e., α, is considered at 5% ($Z_{0.05} = \pm 1.96$), and the cut-off mark for rejecting the null hypothesis is considered as the level of significance (α). The MK test may not represent the actual trend in data when subjected to autocorrelation. Therefore, the modified MK test is applied in this study to estimate the trends to overcome the above-mentioned problem. It is found from the analyses that there is no difference between the original and the modified MK test results (see Supplementary Tables S9 and S10 for the results) in the absence of autocorrelation in the data. Henceforth, the original MK test results are retained here for further discussions for clarity reasons. Figure 2 illustrates the overall methodology of the study.

3. RESULTS

3.1. Model calibration and validation

The SWAT model was calibrated using the SWAT-CUP tool (version 5.1.6) using various optimization techniques and to analyse the uncertainty in the simulations. The ArcSWAT model was then calibrated with the Sequential Uncertainty Fitting (SUFI-2) optimization technique (Khalid *et al.* 2016). In SUFI-2, parameter uncertainty accounts for that in all sources, such as the inaccuracies in driving variables (e.g., rainfall), conceptual model, parameters and measurements. The degree to which all uncertainties are accounted for is quantified by a measure referred to as the *P*-factor, which is the percentage
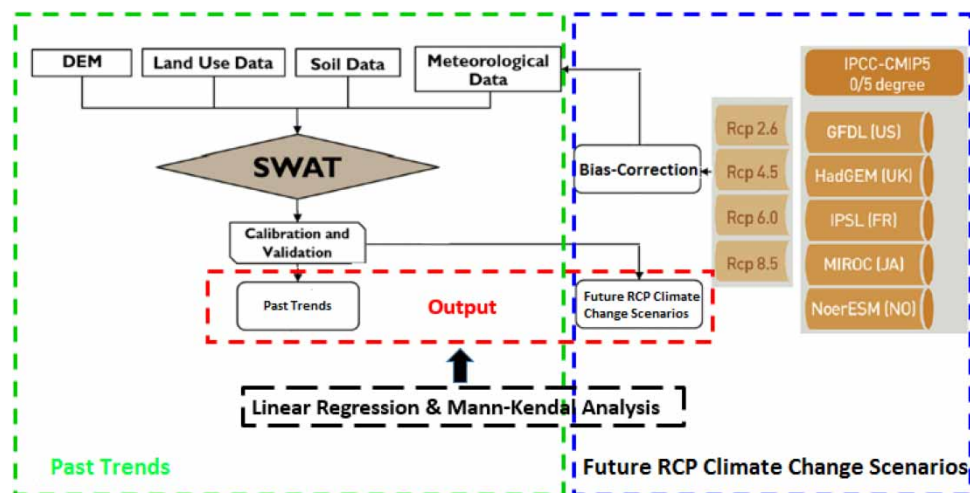

Figure 2 | Methodology adopted for SWAT model runs and GCM bias correction. The input and output data of SWAT model runs are also illustrated.

of data bracketed by the 95% prediction uncertainty (95PPU). The goodness of calibration and prediction uncertainty were determined on the basis of the closeness of the *P*-factor to 100% (i.e., all observations bracketed by the prediction uncertainty) and the *R*-factor to 1 (i.e., achievement of rather small uncertainty band). The model was calibrated and validated with daily and monthly streamflow time series once the major calibration parameters were identified utilizing the Latin hypercube one-factor-at-a-time (LH-OAT) technique (van Griensven *et al.* 2006).

3.1.1. Daily time step

Figure 3 illustrates the output of daily calibration and sensitivity analysis using the SUFI-2 optimization technique. During the periods of calibration and validation, *NSE* values are 0.54 and 0.52, respectively, revealing the model performance to be satisfactory. Similarly, R^2 values of 0.55 and 0.72 for calibration and validation demonstrate a strong correlation between the observed streamflow and its simulated counterpart. The value of the PBIAS for the calibration period is found to be +21.6, whereas it is +22.3 for the validation period, signifying that it lies between the model acceptance criteria defined by Moriasi *et al.* (2007). After sensitivity analysis, 13 most sensitive parameters with considerable effects on streamflow simulation are identified, as shown in Supplementary Table S4 for the daily time step. The actual BF from the observed streamflow using a digital recursive filter is estimated and an illustration is made, from which the NSE is found to be 0.62. The value of the NSE is under the satisfactory limit for model results, as demonstrated in Figure 4.
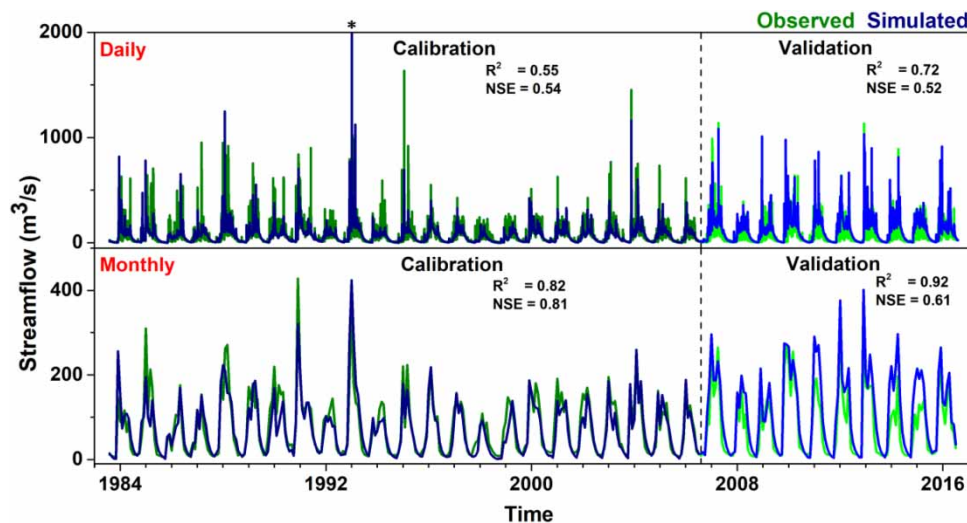

Figure 3 | Observed and simulated daily (upper panel) and monthly (bottom panel) streamflow hydrographs for the calibration and validation periods.
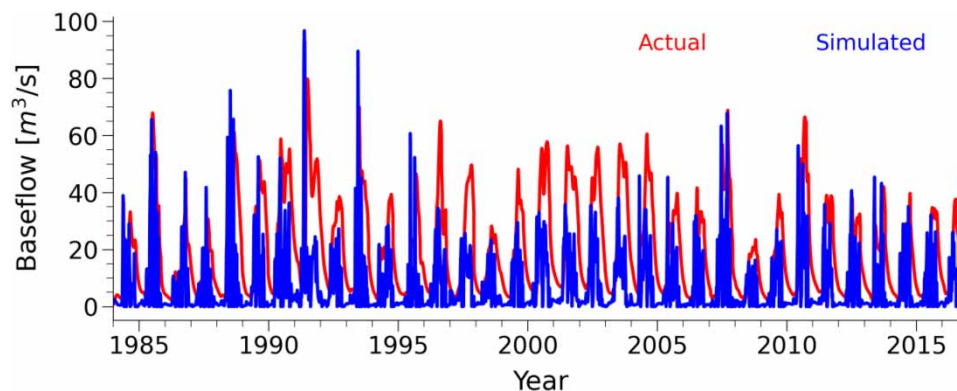

Figure 4 | Actual and simulated BF in the study region.

3.1.2. Monthly time step

Similar to the daily time step, NSE values of 0.81 and 0.61 are obtained during the calibration and validation periods for the monthly time step. On the other hand, R^2 values for the calibration and validation periods are 0.82 and 0.92, respectively, as shown in Figure 3, which demonstrates a better correlation for the monthly than daily time step between observed and simulated streamflow. This improvement in the monthly-scale streamflow is due to a reduction of bias in the streamflow data. The value of the PBIAS was +15.7 for the monthly calibration and +18.4 for the validation. The most influential parameters obtained during the sensitivity analysis for the monthly time steps are listed in Supplementary Table S4.

Thirteen most sensitive parameters are found to be similar for both time steps (Supplementary Table S4), i.e., for daily and monthly. While comparing the sensitivity analysis outcomes of daily and monthly time step simulations, it can be inferred that in the case of the monthly time step, two additional parameters, i.e., 'R__MSK_CO1.bsn' and 'R__MSK_CO2.bsn' (Muskingum Routing Cofficient_1 and Coefficient_2, respectively), are significant. The rank of the rest of the parameters varies for both daily and monthly time steps. Additionally, ranking is performed on the absolute *t*-value, and the parameter with the highest rank affects the streamflow the most. A multiple linear regression analysis is used to find the *t*-statistics of parameter sensitivity. It is a measure of the precision with which the regression coefficient is measured. It is given by

$$t-stat = \frac{\text{Coefficient of parameter}}{\text{Standard error}}$$

On the other hand, 'R_CN2.mgt' is found to be the most sensitive parameter as it ranks 1 for both time steps during sensitivity analysis. The initial SCS runoff curve number for antecedent moisture condition II (R_CN2.mgt) is a function of soil permeability, land use and soil water condition. For monthly calibration, the routing method plays an important role, and, thus, R_MSK_CO1.bsn is one of the important parameters in this regard. Therefore, the Muskingum routing coefficient also controls the catchment runoff characteristics to a great extent. This suggests that this method can be applied for the calibration in the mountainous regions. Furthermore, corresponding to curve number and routing parameter, the main channel Manning's roughness coefficient (V_CH_N2.rte) is identified as another major sensitive parameter. The overall catchment characteristics are, therefore, governed by the surface runoff calibration parameter, but the surface runoff plays a big role in deciding the catchment hydrology. The two additional parameters, i.e., R_MSK_CO1.bsn and R_MSK_CO2.bsn, are found as the sensitive parameters based on the method of routing selected. The method selected corresponds to the Muskingum method of flow routing. In the case of daily streamflow simulation, the variable storage routing approach is more appropriate as opposed to the Muskingum method. Therefore, the two sensitive parameters chosen for the monthly-scale simulation are not considered in the daily-scale simulation.

3.2. Quantification of hydrological fluxes

3.2.1. Past trends

3.2.1.1. Monthly Analysis. All five hydrological fluxes are analysed in monthly time step for the period 1985–2013 and the trends are presented in Supplementary Table S5. A decreasing trend is noticed for discharge flux during the whole study period (Supplementary Figure S2(a)). However, the trend is statistically significant in February and November, but is insignificant in other months. The decreasing trend of streamflow across all analysis periods can be attributed to a reduction in precipitation estimates during the same periods. However, the beginning of summer and the end of monsoon periods experience severe scarcity in water, which causes a decreasing trend in streamflow in February and November. July is the beginning of the monsoon season in the region, resulting in increased water availability for crop growth, and, thus, makes a positive trend in ET. However, the kharif crop growing season is June–September and October is the harvesting period. Henceforth, the magnitude of ET is lower during the period and shows a decreasing trend (Supplementary Figure S2(b)). However, increased water availability and the presence of vegetation in the croplands contribute to a significant positive trend of ET in July and November.

The result for the BF (Supplementary Figure S2(c)) shows positive trends in July, August and September during the peak monsoon period. Conversely, a negative trend is estimated in June due to a delayed monsoon onset rainfall in the study area. The BF shows a decreasing trend in the remaining period, but is statistically insignificant. Furthermore, it is evident from Supplementary Figures S2(d) and S2(e) that SAR and DAR follow a similar pattern of temporal trends, i.e., positive trends in July and September (Supplementary Table S5).

3.2.1.2. Seasonal analysis. Similar to monthly analysis, all fluxes are analysed on a seasonal basis as per IMD classification – pre-monsoon (MAM), monsoon (JJAS), post-monsoon (OND) and winter (JF) – for the study period 1985–2013. Table 1 illustrates the results of the trend analysis of different fluxes for seasonal average. For instance, the discharge decreases in all four seasons, which can be due to the overall decrease in the precipitation in the region. However, the trend is statistically significant in the winter, monsoon and post-monsoon periods (Supplementary Figure S3(a)). The ET and BF show negative trends in all seasons but are statistically insignificant (Supplementary Figures S3(b) and S3(c)). Relatively low rainfall causes unsaturated soil, which provides a lower BF contribution to groundwater and, thus, exhibits a negative trend throughout the analysis period. The presence of forest land significantly affects the BF and ET dynamics in a catchment. As the study area includes more than 60% of land under forest cover, the increased ET dynamics is well reflected in the model results. Additionally, the presence of forest land favours increased infiltration capacity, promoting an increased BF to the catchment. Henceforth, the land-use characteristics are well reflected in the model simulations.

On the other hand, SAR and DAR follow a similar trend (Supplementary Figures S3(d) and S3(e)). The trend observed is positive in monsoon, but negative in the other seasons. This suggests that the maximum amount of groundwater recharge takes place only during the monsoon season for both aquifers in the study area. However, all trends for both fluxes are statistically insignificant (Table 1).

3.2.1.3. Annual analysis. Table 1 and Supplementary Figure S4 illustrate the results of annual average data and they show that the trend for different hydrological fluxes is negative for the study period. Nevertheless, the Q flux is found to be statistically significant. The remaining fluxes, i.e., ET, BF, SAR and DAR, also show decreasing trends but are statistically insignificant. The decreasing trend of Q is likely to intensify further in the form of reduced water availability, which will adversely affect agricultural activities during the non-monsoon periods. Due to alternative dry spells and flash flood–induced instantaneous inundation in the monsoon season, crops are likely to experience severe moisture stress. The substantial increase in ET during the lean periods necessitates frequent irrigation. The contribution of BF is highly warranted to maintain environmental flow in a river, particularly during lean seasons. It is also evident from the analysis that both SAR and DAR are declining, which can lead to a plausible drought condition in the lean periods. Therefore, the construction of an artificial recharge site is very important to enhance both SAR and DAR. The model simulations show that the study area is susceptible to reduced shallow and DAR in future. Therefore, there is a need to adopt some structural measures for enhancing the groundwater recharge, such as the construction of artificial recharge there.

3.2.2. Future RCP climate change scenarios

3.2.2.1. Monthly analysis. All five hydrological fluxes were analysed in monthly time step for the period 2021–2099 and their trends are presented in Supplementary Tables S6(a)–S6(e). For the Q flux, maximum months with a decreasing trend are found with RCP 2.6 of GCM5 and RCP 6.0 of GCM1 during the study period (Supplementary Table S6(a)). On the other hand, increasing trends are estimated for RCP 8.5 in both GCM2 and GCM5 but RCP 6.0 of GCM5 in all months. Six-month positive and negative trends are observed in RCP 8.5 for GCM1 and RCP 6.0 for GCM2. The minimum months that show a decreasing trend are found for the scenario RCP 2.6 of GCM1 and RCPs 4.5 and 6.0 of GCM4. For ET, June–September months show high positive trends (Supplementary Table S6(b)) for all GCMs and RCP scenarios due to the

Table 1 | Trend statistics of annual average, winter, pre-monsoon, monsoon and post-monsoon for different hydrological fluxes during the hindcast period

Hydrological fluxes	Annual average	Season			
		Winter	Pre-monsoon	Monsoon	Post-monsoon
Q (m³s⁻¹/year)	**−1.437 + 1.393**	**−0.394 + 0.353**	−2.023 + 2.946	**−1.467 + 1.453**	**−1.495 + 1.412**
ET (mm/year)	−1.542 + 1.958	−0.101 + 0.164	−0.212 + 0.400	−0.113 + 0.338	−0.083 + 0.111
BF (mm/year)	−1.007 + 3.278	−0.042 + 0.096	−0.102 + 0.219	−0.006 + 0.544	−0.198 + 0.455
SAR (mm/year)	−1.146 + 3.017	−0.051 + 0.092	−0.140 + 0.326	0.020 + 0.504	−0.235 + 0.336
DAR (mm/year)	−0.057 + 0.151	−0.003 + 0.005	−0.007 + 0.016	0.001 + 0.025	−0.012 + 0.017

The bold entries indicate that the trend is statistically significant at the 5% level.

influence of monsoon rainfall. The highest decreasing trends with all GCMs are estimated for May and December, whereas other GCMs show mixed results, i.e., both positive and negative trends.

The results for BF (Supplementary Table S6(c)) show positive trends in all months for the RCP 8.5 scenario in both GCM2 and GCM5. Nevertheless, January, February, March, April, September and December show decreasing trends in most scenarios, while June and October show increasing trends in most GCMs and the RCP scenarios. In addition, RCP 6.0 of GCM1, RCP 8.5 of GCM3 and RCP 2.6 of GCM5 are observed to have a greater number of months with decreasing trends and follow similar trends. Furthermore, it is evident from Supplementary Tables S6(d) and S6(e) that SAR and DAR follow a similar pattern of trends, i.e., increasing trends in June, July and August for most RCPs and GCMs. In addition, RCP 8.5 of GCM2 and GCM5 show a positive trend in all months. However, RCP 6.0 of GCM1, RCP 8.5 of GCM3 and RCP 2.6 of GCM5 show a negative trend in most months. On the other hand, some RCP scenarios in a few GCMs show a zero trend in January, February and December, suggesting that the recharge is equal to discharge during that period. Vegetation is one of the fundamental components in the hydrological cycle that can alter the fluxes through ET. However, our study focused on the future projections here and assumed that the land-use characteristics and the crop calendar will remain constant in the analysis period. In addition, being a mountainous catchment, the study area is subjected to minimal alteration in land use. The crop calendar and its respective management practices are simulated with the crop management module of SWAT and are updated accordingly for different crop growing seasons.

3.2.2.2. Seasonal analysis. Supplementary Tables S7(a)–S7(e) illustrate the results of the trend analyses of different fluxes for each season. The GCMs show decreasing trends during the winter, pre-monsoon and post-monsoon seasons for streamflow in most RCP scenarios. However, during the monsoon season, very few RCP scenarios are found to be negative (Supplementary Figure S5(a)), indicating floods during the season. On the other hand, all RCP scenarios show positive trends during the monsoon season (Supplementary Figure S5(b)) for ET, which suggests an increase in temperature during this season. Conversely, the highest negative trend of ET is observed during the post-monsoon (Supplementary Table S7(b)) and winter seasons due to infrequent rainfall in these periods. The BF shows the highest negative trend in different RCPs during the pre-monsoon season, followed by winter and post-monsoon seasons (Supplementary Table S7(c)) because of the high amount of water from the ground absorbed by plants and less moisture within the soil. The highest positive trends are estimated in the monsoon season as it receives more rainfall compared to that in other seasons (Supplementary Figure S5(c)). SAR and DAR follow a similar trend (Supplementary Figures S5(d) and S5(e)). That is, the RCP scenarios show positive trends mostly for the monsoon and negative for other seasons. This indicates that peak groundwater recharge takes place only during the monsoon season for both aquifers. In addition, all trend values in DAR are smaller than those in SAR (Supplementary Table S7(e)).

3.2.2.3. Annual Analysis. Figure 5 and Supplementary Table S8 illustrate the results of annual analysis using different GCMs and RCP scenarios for the period 2021–2099. It is revealed that all five hydrological fluxes exhibit a positive trend in GCM4 (Supplementary Figure S6(d)) for all RCP scenarios. On the other hand, in GCM1, two of the RCPs show a positive trend, i.e., RCP 2.6 and RCP 4.5, whereas RCP 6.0 shows a negative trend (Supplementary Figure S6(a)). The ET in RCP 8.5 of GCM1 (Supplementary Table S8) shows an increasing trend, but the rest of the fluxes show decreasing trends. In the case of GCM2, only the Q flux in RCP 6.0 shows a negative trend, whereas positive trends are estimated for other fluxes in the remaining RCPs. Similar to GCM2, a reverse scenario is observed in GCM5 of RCP 2.6, where the ET flux is positive and the rest of the fluxes are negative. Furthermore, three fluxes related to groundwater flow, i.e., BF, SAR and DAR, show a decreasing trend in RCP 8.5 of GCM3 (Supplementary Table S8), but increasing trends are found for the remaining fluxes and other RCPs.

4. DISCUSSION AND CONCLUSION

The findings of multi-temporal trend analysis used here reveal that the magnitude and direction of trends are highly dependent on the length of data and the position of sub-series within the time series. A streamflow trend analysis by Birsan *et al.* (2005) in the mountainous regions of Switzerland for the period 1931–2000 showed that mountainous basins are more vulnerable to environmental alteration and, thus, to climate change. This is consistent with the findings by Beniston (2003), in which the importance and necessity of more research and policy formulation on environmental change in global mountainous river
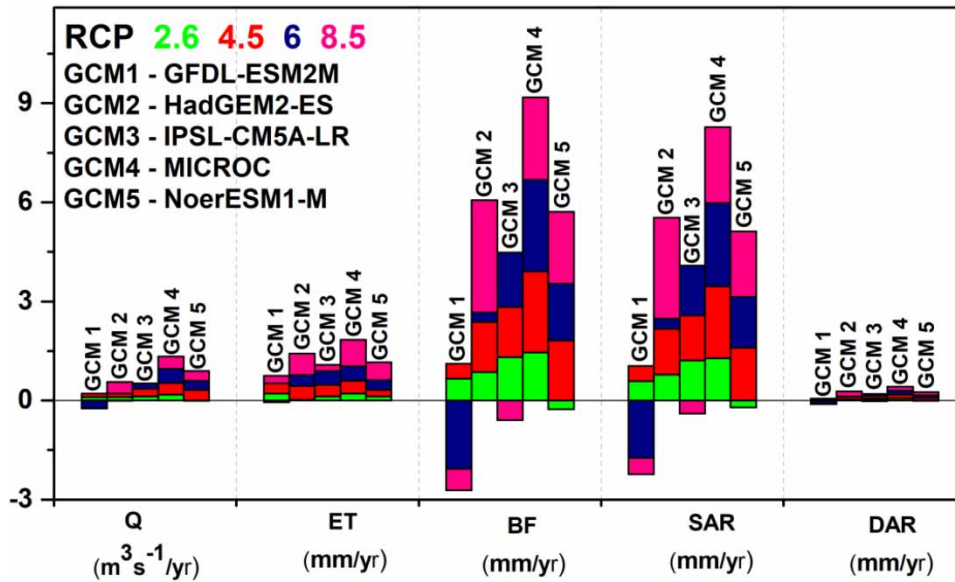
Figure 5 | Annual trends for different hydrological fluxes for different RCP scenarios over the study area. The names of all five GCMs are also shown in the figure.

basins are emphasized. In general, two aspects of catchment differ significantly in the mountain regions: the BF and precipitation characteristics. The BF contribution in mountainous regions is very high, which results in more discharge. To deal with this situation, the calibration of BF is performed more carefully with respect to the observed BF, leading to more realistic estimates of streamflow. Furthermore, the mountainous regions are susceptible to orographic precipitation and its magnitude also changes with different elevations of the terrain. This has been conceptualized in the SWAT model by means of elevation bands, by which the dynamics of hillslope can be accommodated in the model with reasonable accuracy.

The simulated annual, seasonal and annual maximum streamflow of the Brahmaputra River Basin is projected to increase in the future for 18 diversified climate change scenarios (Alam *et al.* 2021). The SWAT model used in a mountainous watershed of Nepal to evaluate its potential in hydrological application found that the 'ALPHA_BF' (BF recession α-factor) was the most sensitive model parameter in streamflow simulation, as found in our study for the MDRB (e.g., Dhami *et al.* 2018). Furthermore, Immerzeel *et al.* (2013) used the results of an ensemble of climate model simulations and a glacio-hydrological model simulation to examine the influence of climate change on the hydrology of two Himalayan watersheds, i.e., the Baltoro (Indus) and Langtang (Ganges), and showed an increase in streamflow in both watersheds for future scenarios, as for MDRB. The uncertainty in the future streamflow projections was due to changes in the precipitation simulations by the models. A study for the Zagros Mountain of Iran by Masih *et al.* (2010) showed increasing and decreasing trends of streamflow during the post-monsoon and lean periods, respectively, which is in accordance with the findings of our study.

We used a common approach to quantify the implications of climate change on streamflow in the MDRB by utilizing bias-corrected multiple GCM results and the SWAT model. Therefore, the evaluations can be enhanced further by considering the effects of changes in land use. In addition, there may be uncertainties associated with the model simulations and the bias-correction method, which can be improved in future simulations and analyses. The following conclusions are drawn from the analyses.

(i) The model performed relatively better in monthly time steps over daily time steps. The streamflow shows a decreasing trend for all months with statistically significant trends in February and November. An insignificant increase in ET is noticed for July and November. A positive trend is estimated for Q during the monsoon period. DAR and SAR also exhibit positive trends during July and September.

(ii) The streamflow exhibits a decreasing trend in all seasons. However, the trend is significant only for the post-monsoon period. ET and BF also exhibit a decreasing trend in all seasons. Insignificant positive trends are found for both SAR and DAR in the monsoon season.

(iii) For future projections, the months January, February and March show the highest decreasing trends in all GCMs, but the highest increasing trend is in September for streamflow. For ET, the June–September period shows the highest positive trends, but the peak negative trend is in May and December for GCMs and RCP scenarios. Since it is difficult to accurately predict the future evolution of vegetation and LULC in the study region, the projected changes in hydrological fluxes by the models will have an uncertainty based on this. Therefore, care must also be taken when interpreting future projections.

In summary, the declining trend of streamflow may trigger water scarcity in the region, which will adversely affect drinking water and agriculture activities during the non-monsoon periods. Since crops are projected to experience moisture stress due to prolonged dry spells, irrigation is essential during the non-monsoon periods. Therefore, water resources management is highly warranted for ensuring sustainable crop production in order to meet the food demands of a growing population. This systematic multi-temporal analysis for the MDRB will provide a better planning framework for river basin management in mountainous regions and for policy formulation.

AUTHORS' CONTRIBUTIONS

S.M. conceptualized the original draft, prepared its methodology, performed validation, investigation, data curation and visualization and also wrote the original draft; S.R., S.S.D. and R.M. were involved in the preparation of the methodology of the original draft, validation, investigation, data curation, visualization and writing of the original draft; J.K. conceptualized the original draft, prepared its methodology, performed investigation and visualization and wrote the original draft; he also reviewed and edited the draft and was involved in supervision and funding acquisition; and M.K.J. was involved in preparing the methodology of the original draft, investigation, writing, supervision and funding acquisition.

CODE AVAILABILITY

The codes are available upon request.

CONFLICT OF INTEREST

On behalf of all the authors, the corresponding author states that there is no conflict of interest.

DATA AVAILABILITY STATEMENT

The datasets used in the study are available on the following domains. IMD Rainfall: https://www.imdpune.gov.in/Clim_-Pred_LRF_New/Grided_Data_Download.html, LULC data: https://www.esa-landcover-cci.org/, and GCM results: https://www.2w2e.com/home/CIMP. Other data are available on request.

REFERENCES

Alam, S., Ali, M. M., Rahaman, A. Z. & Islam, Z. 2021 Multi-model ensemble projection of mean and extreme streamflow of Brahmaputra River Basin under the impact of climate change. *Journal of Water and Climate Change* **12** (5), 2026–2044. https://doi.org/10.2166/WCC.2021.286.

Arnold, J. G., Allen, P. M. & Bernhardt, G. 1993 A comprehensive surface-groundwater flow model. *Journal of Hydrology* **142** (1–4), 47–69. https://doi.org/10.1016/0022-1694(93)90004-S.

Arnold, J. G., Muttiah, R. S., Srinivasan, R. & Allen, P. M. 2000 Regional estimation of base flow and groundwater recharge in the Upper Mississippi river basin. *Journal of Hydrology* **227** (1–4), 21–40. https://doi.org/10.1016/S0022-1694(99)00139-0.

Beniston, M. 2003 Climatic change in mountain regions: a review of possible impacts. *Climatic Change* **59** (1), 5–31. https://doi.org/10.1023/A:1024458411589.

Bhattacharya, B. 2017 *Fluvial Dynamics and Their Impact on Land Use of Manu deo River Basin Tripura with Emphasis on Fatikroy Kumarghat Area*. Tripura University, Agartala, India.

Birsan, M. V., Molnar, P., Burlando, P. & Pfaundler, M. 2005 Streamflow trends in Switzerland. *Journal of Hydrology* **314** (1–4), 312–329. https://doi.org/10.1016/J.JHYDROL.2005.06.008.

Choudhury, B. U., Das, A., Ngachan, S. V., Slong, A., Bordoloi, L. J. & Chowdhury, P. 2012 Trend analysis of long-term weather variables in mid-altitude Meghalaya, North-East India. *Journal of Agricultural Physics* **12** (1), 12–22.

Dash, S. S., Sahoo, B. & Raghuwanshi, N. S. 2019 A SWAT-Copula based approach for monitoring and assessment of drought propagation in an irrigation command. *Ecological Engineering* **127**, 417–430. https://doi.org/10.1016/J.ECOLENG.2018.11.021.

Dash, S. S., Sena, D. R., Mandal, U., Kumar, A., Kumar, G., Mishra, P. K. & Rawat, M. 2021 A hydrological modelling-based approach for vulnerable area identification under changing climate scenarios. *Journal of Water and Climate Change* **12** (2), 433–452. https://doi.org/10.2166/WCC.2020.202.

Dhami, B., Himanshu, S. K., Pandey, A. & Gautam, A. K. 2018 Evaluation of the SWAT model for water balance study of a mountainous snowfed river basin of Nepal. *Environmental Earth Sciences* **77** (1), 1–20. https://doi.org/10.1007/S12665-017-7210-8.

Dhar, S. & Mazumdar, A. 2009 Hydrological modelling of the Kangsabati river under changed climate scenario: case study in India. *Hydrological Processes* **23** (16), 2394–2406. https://doi.org/10.1002/HYP.7351.

Fiseha, B. M., Setegn, S. G., Melesse, A. M., Volpi, E. & Fiori, A. 2014 Impact of climate change on the hydrology of Upper Tiber River Basin using bias corrected regional climate model. *Water Resources Management* **28** (5), 1327–1343. https://doi.org/10.1007/S11269-014-0546-X.

Goyal, M. K., Shivam, Sarma, A. K. & Singh, D. S. 2018 Subansiri: largest tributary of Brahmaputra River, Northeast India. In: *The Indian Rivers* (Sen Singh, D., ed.). Springer, Singapore, pp. 523–535. https://doi.org/10.1007/978-981-10-2984-4_36

Immerzeel, W. W., Pellicciotti, F. & Bierkens, M. F. P. 2013 Rising river flows throughout the twenty-first century in two Himalayan glacierized watersheds. *Nature Geoscience* **6** (9), 742–745. https://doi.org/10.1038/ngeo1896.

Kendall, M. G. 1975 *Rank Correlation Methods*. Griffin, London.

Khalid, K., Ali, M. F., Rahman, N. F. A., Mispan, M. R., Haron, S. H., Othman, Z. & Bachok, M. F. 2016 Sensitivity analysis in watershed model using SUFI-2 algorithm. *Procedia Engineering* **162**, 441–447. https://doi.org/10.1016/J.PROENG.2016.11.086.

Kharin, V. V., Zwiers, F. W., Zhang, X. & Wehner, M. 2013 Changes in temperature and precipitation extremes in the CMIP5 ensemble. *Climatic Change* **119** (2), 345–357. https://doi.org/10.1007/S10584-013-0705-8.

Kusre, B. C., Baruah, D. C., Bordoloi, P. K. & Patra, S. C. 2010 Assessment of hydropower potential using GIS and hydrological modeling technique in Kopili River basin in Assam (India). *Applied Energy* **87** (1), 298–309. https://doi.org/10.1016/J.APENERGY.2009.07.019.

Kuttippurath, J., Murasingh, S., Stott, P. A., Balan Sarojini, B., Jha, M. K., Kumar, P., Nair, P. J., Varikoden, H., Raj, S., Francis, P. A. & Pandey, P. C. 2021 Observed rainfall changes in the past century (1901–2019) over the wettest place on Earth. *Environmental Research Letters* **16** (2), 024018. https://doi.org/10.1088/1748-9326/ABCF78.

Mann, H. B. 1945 Nonparametric tests against trend. *Econometrica* **13** (3), 245. https://doi.org/10.2307/1907187.

Masih, I., Uhlenbrook, S., Maskey, S. & Smakhtin, V. 2010 Streamflow trends and climate linkages in the Zagros Mountains, Iran. *Climatic Change* **104** (2), 317–338. https://doi.org/10.1007/S10584-009-9793-X.

Moriasi, D. N., Arnold, J. G., Van Liew, M. W., Bingner, R. L., Harmel, R. D. & Veith, T. L. 2007 Model evaluation guidelines for systematic quantification of accuracy in watershed simulations. *Transactions of the ASABE* **50** (3), 885–900. https://doi.org/10.13031/2013.23153.

Moss, R. H., Edmonds, J. A., Hibbard, K. A., Manning, M. R., Rose, S. K., Van Vuuren, D. P., Carter, T. R., Emori, S., Kainuma, M., Kram, T., Meehl, G. A., Mitchell, J. F. B., Nakicenovic, N., Riahi, K., Smith, S. J., Stouffer, R. J., Thomson, A. M., Weyant, J. P. & Wilbanks, T. J. 2010 The next generation of scenarios for climate change research and assessment. *Nature* **463** (7282), 747–756. https://doi.org/10.1038/nature08823.

Murasingh, S., Jha, M. K., Dash, S. S. & Jayanarayanan, K. 2018 Evaluation of daily and monthly streamflow simulation for a hilly watershed of North-East India. *AGU Fall Meeting, Washington, D.C.*, 2018, H43E-2434. Available from: https://ui.adsabs.harvard.edu/abs/2018AGUFM.H43E2434M/abstract.

Neitsch, S. L., Arnold, J. G., Kiniry, J. R. & Williams, J. R. 2011 *Soil and Water Assessment Tool Theoretical Documentation Version 2009*. Texas Water Resources Institute Technical Report No. 406.

Padhiary, J., Patra, K. C., Dash, S. S. & Uday Kumar, A. 2020 Climate change impact assessment on hydrological fluxes based on ensemble GCM outputs: a case study in eastern Indian River Basin. *Journal of Water and Climate Change* **11** (4), 1676–1694. https://doi.org/10.2166/WCC.2019.080.

Praskievicz, S. 2018 Downscaling climate-model output in mountainous terrain using local topographic lapse rates for hydrologic modeling of climate-change impacts. *Physical Geography* **39** (2), 99–117. https://doi.org/10.1080/02723646.2017.1378555.

Praskievicz, S. & Bartlein, P. 2014 Hydrologic modeling using elevationally adjusted NARR and NARCCAP regional climate-model simulations: Tucannon River, Washington. *Journal of Hydrology* **517**, 803–814. https://doi.org/10.1016/J.JHYDROL.2014.06.017.

Raneesh, K. Y. & Santosh, G. T. 2011 A study on the impact of climate change on streamflow at the watershed scale in the humid tropics. *Hydrological Sciences Journal* **56** (6), 946–965. https://doi.org/10.1080/02626667.2011.595371.

Singh, O. & Kumar, M. 2013 Flood events, fatalities and damages in India from 1978 to 2006. *Natural Hazards* **69** (3), 1815–1834. https://doi.org/10.1007/S11069-013-0781-0.

Sinha, R. K., Eldho, T. I. & Subimal, G. 2020 Assessing the impacts of land cover and climate on runoff and sediment yield of a river basin. *Hydrological Sciences Journal* **65** (12), 2097–2115. https://doi.org/10.1080/02626667.2020.1791336.

Teutschbein, C. & Seibert, J. 2010 Regional climate models for hydrological impact studies at the catchment scale: a review of recent modeling strategies. *Geography Compass* **4** (7), 834–860. https://doi.org/10.1111/J.1749-8198.2010.00357.X.

Tung, Y.-K. 2005 Uncertainty and reliability analysis. In: *Water Resources Systems Management Tools* (Mays, L. W., ed.). McGraw-Hill, New York.

van Griensven, A., Meixner, T., Grunwald, S., Bishop, T., Diluzio, M. & Srinivasan, R. 2006 A global sensitivity analysis tool for the parameters of multivariable catchment models. *Journal of Hydrology* **324** (14), 10–23.

Varikoden, H. & Revadekar, J. V. 2020 On the extreme rainfall events during the southwest monsoon season in northeast regions of the Indian subcontinent. *Meteorological Applications* **27** (1), e1822. https://doi.org/10.1002/MET.1822.

Verma, A. K. & Jha, M. K. 2015 Evaluation of a GIS-based watershed model for streamflow and sediment-yield simulation in the Upper Baitarani River Basin of Eastern India. *Journal of Hydrologic Engineering* **20** (6). https://doi.org/10.1061/(ASCE)HE.1943-5584.0001134.